

We thank the editor for reporting us the grammatical issues. We revised the manuscript once more correcting the typos and language issues.

Sincerely,

The Corresponding Author

Stefano Urbani

1 **Estimating the depth and evolution of intrusions at resurgent** 2 **calderas: Los Humeros (Mexico)**

3 Stefano Urbani¹, Guido Giordano^{1,2}, Federico Lucci¹, Federico Rossetti¹, Valerio Acocella¹,
4 Gerardo Carrasco- Núñez³

5 ¹Dipartimento di Scienze, Università degli Studi Roma Tre, L.go S.L. Murialdo 1, I-00146 Rome, Italy

6 ²CNR - IDPA c/o Università degli Studi di Milano, Via Luigi Mangiagalli, 34, 20133 Milano

7 ³Centro de Geociencias, Universidad Nacional Autónoma de México, Campus UNAM Juriquilla, 76100, Queretaro,
8 Mexico

9 *Correspondence to:* Stefano Urbani (stefano.urban@uniroma3.it)

10 **Abstract.** Resurgent calderas are excellent targets for geothermal exploration, as they are associated with the shallow
11 emplacement of magma, resulting in widespread and long lasting hydrothermal activity. Resurgence is classically
12 attributed to the uplift of a block or dome resulting from the inflation of the collapse-forming magma chamber due to
13 the intrusion of new magma. The Los Humeros volcanic complex (LHVC; Mexico), consists of two nested calderas: the
14 outer and older Los Humeros formed at 164 ka and the inner, Los Potreros, formed at 69 ka. The latter is resurgent and
15 currently the site of an active and exploited geothermal field (63 MWe installed). Here we aim at better defining the
16 characteristics of the resurgence in Los Potreros, by integrating field work with analogue models, evaluating the spatio-
17 temporal evolution of the deformation and the depth and extent of the intrusions responsible for the resurgence which
18 may also represent ~~also~~ the local heat source(s).

19 Structural field analysis and geological mapping show that the floor of the Los Potreros caldera ~~floor~~ is characterized by
20 several lava domes and cryptodomes (with normal faulting at the top) that suggest multiple deformation sources
21 localized in narrow areas.

22 Analogue experiments are then used to define the possible source of intrusion responsible for the observed surface
23 deformation. ~~The analogue experiments simulate the deformation pattern observed in the field, consisting of magma~~
24 ~~intrusions pushing a domed area developing an apical depression. To define the possible depth of the intrusion~~
25 ~~responsible for the observed surface deformations, We~~ apply a tested relationship between the surface deformation
26 structures and depth of elliptical sources ~~relations for elliptical sources~~ to our experiments with sub-circular sources. We
27 found that ~~these~~ this ~~relationship is~~ are independent of the source and surface dome eccentricity and suggest that the
28 magmatic sources inducing the deformation in Los Potreros are located at very shallow depths (hundreds of meters),
29 which is in agreement with the well data and field observations. We propose that the recent deformation at LHVC is not
30 a classical resurgence associated with the bulk inflation of a deep magma reservoir; rather ~~this~~ it is related to the ascent
31 of ~~shallow (<1 km)~~ multiple magma bodies at shallow crustal conditions (< 1 km depth). A similar multiple source
32 model of the subsurface structure has been also proposed for other calderas with an active geothermal system (Usu
33 volcano, Japan) suggesting that the model proposed may have wider applicability.

34 **1 Introduction**

35 Caldera resurgence consists of the post-collapse uplift of part of the caldera floor. Resurgence has been described in
36 several calderas worldwide (Smith and Bailey, 1968; Elston, 1984; Lipman, 1984 and references therein), representing a
37 frequent step in caldera evolution. Several mechanisms that trigger resurgence have been invoked, including the
38 pressurization of the hydrothermal system (Moretti et al., 2018), regional earthquakes (Walter et al., 2009), and

39 magmatic intrusion (Kennedy et al. 2012). Discriminating the contributions to the observed uplift of each of these
40 mechanisms is often challenging (Acocella, 2014). However, despite the possible hydrothermal and tectonic
41 contributions, field observations in eroded resurgent calderas (e.g. Tomochic, Swanson and McDowell, 1985; Kutcharo,
42 Goto and McPhie 2018; Turkey Creek, Du Bray and Pallister, 1999) coupled with the long timescale of the uplift of the
43 caldera floor (from tens to thousands of years), suggest that the intrusion of magmatic bodies is the prevalent
44 mechanism for resurgence.

45 Resurgence is commonly attributed to the emplacement of silicic magmas at different depth levels under limited
46 viscosity contrasts with regard to the previously emplaced magma (Marsh, 1984; Galetto et al., 2017). However, though
47 rare, resurgence may be also triggered by the injection of more primitive magma (Morán-Zenteno et al., 2004; Kennedy
48 et al., 2012) or by the emplacement of basaltic sills, as recently documented at the Alcedo caldera (Galapagos; Galetto
49 et al., 2019). The shape of the intracaldera resurgent structures is variable, being characterized by elliptical domes with
50 longitudinal graben(s) at the top (e.g. Toba; De Silva et al., 2015; Snowdonia, Beavon, 1980; Timber Mountain,
51 Christiansen et al., 1977) or, less commonly, by sub-circular domes (e.g. Cerro Galan, Folkes et al., 2011; Long Valley,
52 Hildreth et al., 2017; Grizzly Peak, Fridrich et al., 1991) with both longitudinal grabens (Long Valley) or concentric
53 fault blocks (Grizzly Peak) at their top.

54 Whatever is the shape, resurgence is often associated with hydrothermal and ore forming processes, since the circulation
55 pattern and temperature gradients of geothermal fluids are structurally-controlled by the space-time distribution of faults
56 and fractures and by the depth and shape of the magmatic sources (e.g. Guillou Frottier et al., 2000; Prinbow et al.,
57 2003; Stix et al., 2003; Mueller et al., 2009; Giordano et al., 2014; [Kennedy et al., 2018](#)). Therefore, the characterisation
58 of the magma that drives resurgence (location, depth and size) and of the factors controlling the release of heat
59 (permeability, fracture patterns, and fluid flow) have important implications for the exploration and exploitation of
60 renewable geothermal energy resources. In particular, the estimation of the location, depth and geometry of the
61 magmatic sources is crucial to define the geothermal and mineral potential of resurgent calderas, allowing an
62 economically sustainable exploration and exploitation of their resulted natural resources.

63 The depth and size of the magmatic sources influence the deformation style of the resurgence at the surface (Acocella et
64 al., 2001). Deep sources (i.e. depth/diameter ratio ~ 1 assuming a spherical source) are associated ~~to~~with resurgent
65 blocks (e.g. Ischia and Pantelleria, Acocella and Funiciello, 1999; Catalano et al., 2009), whereas shallower sources (i.e.
66 depth/diameter ratio ~ 0.4) to resurgent domes (e.g. Valles and Yenkahe, Kennedy et al., 2012; Brothelande et al., 2016).
67 Moreover, uplift rates may change by one order of magnitude from ~ 1 to ~ 10 cm per year (e.g. Yellowstone and Iwo
68 Jima, Chang et al., 2007; Ueda et al., 2018). Nevertheless, despite showing different uplift styles and rates, these natural
69 examples share a common feature that is a coherent uplift of the caldera floor. A different style of deformation is
70 observed at calderas characterized by the widespread and delocalized uplift of several minor portions of the caldera
71 floor, associated with the shallow emplacement of ~~sills~~ and cryptodomes, as observed at Usu volcano (Japan,
72 Matsumoto and Nakagawa, 2010; Tomya et al., 2010). Such deformation pattern suggests different depth(s) and
73 extent(s) of the magma source(s). A better assessment of the subsurface structure in this type of calderas has crucial
74 implications for geothermal exploration.

75 The Los Humeros Volcanic Complex (LHVC, Mexico) is an important geothermal target area, consisting of two nested
76 calderas: Los Humeros (the outer, larger and older one; 164 ka) and Los Potreros (the inner, smaller and younger one;
77 69 ka) (Fig. 1). The latter is characterized by the resurgence of its floor, interpreted to be due to the inflation of the
78 magma chamber responsible for the collapse, with its top at ca 5 km depth (Norini et al., 2015, 2019).

79 This paper aims ~~at to~~ (1) evaluating the depth of the intrusion(s) inducing the uplift in the LHVC area; (2) explain the
80 spatio-temporal evolution of the observed deformation of the caldera floor; and (3) test the validity of the linear
81 relationship between the surface deformation structures and depth of elliptical sources (Brothelande and Merle 2015)
82 for sub-circular sources. To achieve these goals, we integrate results from structural field investigations carried out
83 within the Los Potreros caldera with those derived from analogue experiments specifically designed to constrain the
84 depth of the deformation source(s) in volcanic caldera environments. The obtained results show that: (1) the relation
85 between the source depth and surface deformation structures is independent of the source eccentricity; (2) the LHVC is
86 characterized by discontinuous and small-scale (areal extent $\sim 1 \text{ km}^2$) surface deformations generated from multiple and
87 shallow-emplaced ($< 1 \text{ km}$ depth) magmatic bodies. These results should be taken into account for the planning of
88 future geothermal operations at the LHVC and in other calderas showing similar surface deformation.

89 2 Geological-structural setting

90 LHVC is located at the eastern termination of the Trans Mexican Volcanic Belt (TMVB, see inset in Fig. 1). The TMVB
91 is the largest Neogene volcanic arc in Mexico ($\sim 1000 \text{ km}$ long and up to $\sim 300 \text{ km}$ wide), commonly associated with the
92 subduction of the Cocos and Rivera plates beneath the North American plate along the Middle American trench (Ferrari
93 et al., 2012, and references therein). The LHVC consists of two nested calderas formed during the Pleistocene: the outer
94 $18 \times 16 \text{ km}$ Los Humeros caldera and the inner $10 \times 8 \text{ km}$ Los Potreros caldera (Fig. 1, Ferriz and Mahood, 1984;
95 Norini et al., 2015; Carrasco-Núñez et al., 2017b).

96 Based on updated stratigraphic and geochronological information, the evolution of the LHVC can be divided into three
97 main eruptive stages (Table 1, Carrasco-Núñez et al., 2017b, 2018). Pre-caldera volcanism extended between ca. 700
98 and 164 ka (zircon U-Th and feldspar $^{39}\text{Ar}/^{40}\text{Ar}$ ~~ages, datings in~~ Carrasco-Núñez et al., 2018), showing evidence for an
99 extended building phase leading to the establishment of the large volume rhyolitic reservoir, which fed several lava
100 domes erupted to the western border of the Los Humeros Caldera. A Caldera stage started at ca. 164 ka (zircon U-Th
101 and feldspar $^{39}\text{Ar}/^{40}\text{Ar}$ ages, Carrasco-Núñez et al., 2018), with the eruption of the $>115 \text{ km}^3$ (dense rock equivalent
102 volume) Xaltipan ignimbrite that triggered the collapse of the Los Humeros caldera. This was followed by a Plinian
103 eruptive episodic sequence, characterized by the emplacement of several rhyodacitic pumice fallout layers grouped as
104 the Faby Tuff (Ferriz and Mahood, 1984). The Caldera stage ended with the eruption of the 15 km^3 (dense rock
105 equivalent volume) Zaragoza rhyodacite-andesite ignimbrite at $69 \pm 16 \text{ ka}$ (feldspar $^{39}\text{Ar}/^{40}\text{Ar}$ ages, Carrasco-Núñez et
106 al., 2018) associated with the collapse of the nested Los Potreros caldera.

107 A post-caldera stage ($< 69 \text{ ka}$) is interpreted by Carrasco-Núñez et al. (2018) as composed by two main eruptive phases:
108 (i) a late Pleistocene resurgent phase, characterized by the emplacement of silica-rich small domes and disperse
109 explosive activity within Los Potreros caldera, followed by (ii) Holocene basaltic to trachytic monogenetic volcanism
110 both inside and at the caldera-rim. This eruptive behaviour indicates a change in the configuration of the magmatic
111 plumbing system compared to the caldera stage of Los Humeros, when a single, large and homogenized magma
112 reservoir was in existence (e.g. Ferriz and Mahood, 1984; Verma, 1985). Volcanological and petrological data indicate
113 that the post-caldera volcanism is associated with a heterogeneous multi-layered system vertically distributed within the
114 crust, with a deep (ca. 30 km depth) basaltic reservoir feeding progressively shallower and smaller distinct stagnation
115 layers, pockets and batches up to very shallow conditions (ca. 3km) (Lucci et al., 2020), in agreement with recent
116 conceptual models for magma reservoirs under caldera systems (e.g. Cashman and Giordano, 2014).

117 During the early resurgent phase of the post-caldera stage, rhyolitic domes were emplaced along the northern rim and
118 within the Los Humeros caldera. Available ages span between $44.8 \pm 1.7 \text{ ka}$ (zircon U-Th dating ages) and $50.7 \pm 4.4 \text{ ka}$

119 (~~feldspar ³⁹Ar/⁴⁰Ar dating ages~~), (Carrasco-Núñez et al., 2018). This effusive activity was followed by several
120 explosive eruptions, which originated a dacitic air fall called Xoxoctic Tuff (0.6 km³, Ferriz and Mahood, 1984) and a
121 pyroclastic sequence that includes an explosive breccia and pyroclastic flow deposits comprising the Llano Tuff (Ferriz
122 and Mahood 1984; Willcox, 2011).

123 The Holocene ring-fractures fed bimodal magmatism characterized by both explosive and effusive activity, producing
124 several lava flows and domes, as well as the ca. 7 ka (C-14 age, Dávila-Harris and Carrasco-Núñez, 2014) Cuicuiltic
125 Member during periods of dominant explosive activity. The Cuicuiltic Member consists of alternating pumices and
126 scoriae erupted during contemporaneous sub-Plinian to Strombolian activity from multiple vents located mostly along
127 the inner part of the caldera and outer caldera ring faults (Dávila-Harris and Carrasco-Núñez, 2014). During this phase,
128 less evolved lavas (trachyandesite to basalt) were erupted within and outside the Los Potreros caldera, including the
129 olivine-bearing basaltic lava that fills the previously formed Xalapasco crater (Fig. 1). Trachytic lava flows are the most
130 recent products in the area, with an age of ca. 2.8 ka (C-14 age, Carrasco-Núñez et al., 2017b).

131 The reconstruction of the shallow stratigraphy within the Los Potreros caldera is chiefly derived from the analysis of
132 available well-logs (Figs. 2a-b Carrasco-Núñez et al., 2017a, b). Overall, the post-caldera units are lithologically
133 dominated by lava flows resting on ignimbrite deposits emplaced during the caldera stage. Ignimbrites of the caldera
134 stage rest in turn on a thick sequence dominated by andesite lavas dated at ca. 1.4-2.8 Ma (~~feldspar ³⁹Ar/⁴⁰Ar~~
135 ~~ages dating~~, Carrasco-Núñez et al., 2017a). The subsurface geometry of the pre- and syn-caldera products is shown in
136 Figs. 2a-b, where the in-depth geometry of the different magmatic products ~~are is~~ cross-correlated and projected along
137 the N-S and E-W direction, respectively. The N-S projection shows a constant depth of the top surface of the pre-caldera
138 andesites that is associated with a highly variable depth (down to -400 m) of the top surface of the syn-caldera Xaltipan
139 ignimbrite. The W-E projection shows a higher depth variability of both the top surface of the pre-caldera group (down
140 to -500 m between H-19 and H-25 wells) and that of the Xaltipan ignimbrite (down to -400 m between H-19 and H-10
141 wells). Basaltic and rhyolitic-dacitic lavas occur at various depths (Carrasco-Núñez et al., 2017a); rhyolites-dacites are
142 located mostly at the base (H-20 and H-26 wells) or within (H-05 well) the caldera group or the old andesite sequence
143 (H-25 and H-19 wells). Basalts are located only within the pre-caldera andesite sequence, both at its base (in contact
144 with the limestone basement; H-5 and H-8 wells) and at its top (in contact with the base of the caldera sequence; H-10
145 well). These bimodal lava products, showing an irregular lateral distribution, have been interpreted as subaerial
146 (Carrasco-Núñez et al., 2017a).

147 The structural architecture of the LHVC is controlled by a network of active extensional fault systems, made of NNW-
148 SSE, N-S, NE-SW and E-W striking fault strands cutting across the Los Potreros caldera floor. The following main
149 faults were recognised (Norini et al., 2015, 2019; Calcagno et al., 2018) (Fig.1): (i) Maxtaloya (NNW-SSE striking), (ii)
150 Los Humeros and Loma Blanca (N-S striking), (iii) Arroyo Grande (NE-SW striking), (iv) Las Viboras and Las Papas
151 (E-W striking). Such active fault systems are interpreted as due to the recent/active resurgence of the Los Potreros
152 Caldera. Since the faults do not show continuity beyond the caldera border, their scarps decrease in height towards the
153 periphery of the caldera and the dip-slip displacement vectors show a semi-radial pattern (Norini et al., 2015).

154 The source of the areal uplift has been inferred to be the inflation of a saucer or cup shaped deep magmatic source
155 elongated NNW-SSE, up warping a 8 x 4 km resurgent block, centred in the SE portion of the caldera, delimited to the
156 W by the NNW-SSE main faults, and toward the north, east and south by the caldera rim (Fig.1, Norini et al., 2015,
157 2019).

158 The seismic activity between 1994-2017 is clustered along the Loma Blanca, Los Humeros and Arroyo Grande faults
159 (Lermo et al., 2018; Fig. 1). Most of the earthquakes show a magnitude (M_w) between 1 and 2.5 and have been mainly

160 interpreted as induced by the geothermal exploitation activity (injection of fluids and hydrofracturing; Lermo et al.,
161 2018). -Four major earthquakes ($M_w = 3.2, 3.6, 3.9$ and 4.2 , at a depth of 1, 4, 2.2 and 1.8 km, respectively) have also
162 been reported, with focal depths close to the trace of the active faults (Loma Blanca and Los Humeros, Fig.1). Such
163 major earthquakes have been interpreted as triggered by fault reactivation due to fluid/brine circulation injected from
164 geothermal wells (Lermo et al., 2018).

165 **3 Methods**

166 This study is based on structural field work combined with analogue models aimed at constraining the depth of the
167 deformation sources in the caldera domain. We also tested if the relation that constrains the depth of the source
168 deformation from surface parameters adopting elliptical sources (Brothelande and Merle 2015) is verified also for sub-
169 circular sources.

170 **3.1 Structural field work**

171 Structural field work was carried out on the post-caldera (Late Pleistocene to Holocene) deposits to characterise the
172 surface deformation related to the recent activity of the Los Potreros caldera and constrain the morphotectonic
173 fingerprints of the resurgence to evaluate its source and areal extent. The geometry and distribution of the observable
174 faults and joints were defined at the outcrop scale by measuring their attitudes (strike and dip; right-hand rule) and
175 spacing. Fault kinematics was assessed through classical criteria on slickensides fault surfaces, such as Riedel shears,
176 growth fibres and sheltering trails (Doblas, 1998). The published geological map (Carrasco-Núñez et al., 2017b) and
177 geothermal well data have been used (Carrasco-Núñez et al., 2017a) to correlate the surface structures at a broader
178 scale. The relationships between faulting and alteration have been assessed (e.g. Giordano et al. 2013; Vignaroli et al.
179 2013, 2015).

181 **3.2 Analogue models: experimental set-up and scaling**

182 Five experiments were undertaken to simulate the ascent of a viscous sub-circular intrusion in a brittle overburden to
183 test the validity of existing relationships between the depth of elliptical intrusions and the observed surface deformation
184 (Brothelande and Merle, 2015). The experimental set-up (Fig. 3) consists of a 31×31 cm glass box filled with a sand
185 pack (crust analogue) of variable thickness (T , of 10, 30 and 50 mm, respectively). In each experiment we imposed a
186 layering using a non-cohesive marine sand below a layer of crushed silica sand (grain size = $40\text{-}200 \mu\text{m}$, cohesion = 300
187 Pa), fixing the thickness ratio of the two layers (T_u/T_1) to 1, to simulate the stratigraphy in Los Potreros (stiffer post
188 caldera lava flows above softer and less cohesive ignimbrite deposits emplaced during the caldera collapse stage). At
189 the base of the sand pack, a piston, controlled by a motor, pushes upward the silicone (magma analogue) placed inside a
190 cylinder 8 cm in diameter. The injection rate is fixed for all the experiments to 2 mm/hr and each experiment was
191 stopped at the onset of the silicone extrusion. Both sand and silicone physical properties are listed in Table 2.

192 At the end of each experiment, the surface has been covered with sand to preserve their final topography and was
193 wetted with water for cutting in sections to appreciate the subsurface deformation. Such sections were used to measure
194 the mean dip of the apical depression faults (θ) induced by the rising silicone. A digital camera monitored the top view
195 deformation of each experiment at 0.02 fps and a laser scanner, placed next to the camera, provided high-resolution data
196 (maximum error ± 0.5 mm) of the vertical displacement to measure in detail the geometrical features of the deformation
197 i.e. dome diameter (L_d), apical depression width (L_g) and dome flank mean dip (α). According to the Buckingham-II
198 theorem (Merle and Borgias 1996 and references therein), our models need 7 independent dimensionless numbers to be

199 properly scaled (i.e. 10 variables minus three dimensions; Table 2). Such dimensionless numbers can be defined as the
200 ratios (Π) listed in Table 3. Some values of Π_5 , representing the ratio between the inertial and viscous forces, are very
201 small both in nature and experiments (1.3×10^{-20} and 6.1×10^{-10} , respectively), indicating that the inertial forces are
202 negligible compared to the viscous forces in both cases.

203 **4 Results**

204 **4.1 Structural geology**

205 The outcropping post-caldera lithologies within the Los Potreros Caldera consist of: (1) the Cuicuiltic Member, which
206 blankets most of the surface of the upper half of the studied area; (2) basaltic lava flows filling the Xalapasco crater and
207 the NW portion of the caldera; and (3) trachyandesitic and trachytic lava domes and thick flows extending in the
208 southern half of the caldera and rhyolitic domes in its central part (Fig. 4). Field work documented that the more
209 evolved lavas form five nearly N-S trending elliptical domes, distributed in both sides of the Los Humeros Fault (Figs. 4
210 and 5a): (i) a 2 km long \times 1.2 km wide trachytic dome located to the west of the Maxtaloya and Los Humeros faults, (ii)
211 a 1 \times 0.7 km trachyandesitic dome located in a northeast area of the Maxtaloya fault, and (iii) one trachyandesitic and
212 two obsidian smaller domes (0.4 \times 0.2 km) to the eastern side of the Los Humeros Fault (LH-11 in Fig. 4).

213 Field work concentrated on the three main uplifted areas corresponding to the surface expression of the Loma Blanca,
214 Arroyo Grande and Los Humeros faults (labelled LH1-2, LH9 and LH10 respectively in Fig. 4). The observed
215 structures in these uplifted areas (joints and faults) affect the deposits of the post-caldera phase. Based on field
216 evidence, we also propose a revised interpretation of the surface structures identified by previous studies (Norini et al.,
217 2015, 2019), distinguishing between lineaments (morphological linear scarps, with no measurable fault offsets and/or
218 alteration at the outcrop scale), active and inactive faults, instead associated with measurable fault offsets and with
219 active or fossil alteration, respectively (Fig. 4). We ~~present detail below a description of the~~ main structures mapped in
220 the studied area, highlighting their temporal and spatial relationships with the post-caldera geological formations. We
221 identified two inactive faults (Maxtaloya and Arroyo Grande), a morphological lineament (Las Papas) and two currently
222 active faults (Los Humeros and Loma Blanca).

223 **4.1.1 Las Papas lineament (sites LH-07, LH-08)**

224 The E-W trending Las Papas lineament is localised within the Cuicuiltic Member (LH-07; Fig. 5b). We identified an
225 erosional surface along the scarp, where unaltered and undeformed Cuicuiltic Member rocks rest above the Xoxotic
226 Tuff (LH-08, Fig. 5c). The E-W trending morphological lineament of Las Papas is probably due to differential erosion
227 of the softer layers of the pyroclastic deposits, successively blanketed by the Cuicuiltic Member.

228 **4.1.2 Arroyo Grande (site LH-09) and Maxtaloya scarps**

229 The NE-SW Arroyo Grande scarp (Fig. 6a) exposes strongly altered and faulted (NW striking faults, mean attitude
230 N144°/68°, number of data (n) = 8) lavas and ignimbrites unconformably covered by the unaltered Cuicuiltic Member
231 (Fig. 6b). The offset observed at the outcrop-scale for the single fault strands is ca. 0.5 m, with a dominant normal dip-
232 slip kinematics (pitch angle of the slickenlines ranging 99°-106°). The inferred cumulative displacement at Arroyo
233 Grande is \sim 10 m. Similarly, an outcrop on the Maxtaloya scarp (in front of well H-6) shows altered trachyandesites
234 covered by unaltered Cuicuiltic Member rocks (Fig. 6c).

235 **4.1.3 Los Humeros (site LH-10)**

275 5. Discussion

276 5.1 Interpretation of the analogue experiments

277 The deformation pattern observed in the analogue experiments for thicker overburdens (experiments 3-4 and 5 with
278 $T/D = 0.37$ and 0.63), showing a sub-circular dome and an apical depression, is in agreement with previous analogue
279 experimental results (Acocella et al., 2001; Marti et al. 1994; Walter and Troll 2001). However, for thinner overburdens
280 (exps. 1-2, $T/D = 0.12$), we observed a new deformation pattern at the surface consisting of an annular peripheral
281 depression due to the rising of the silicone at the edge of the cylinder rather than its centre. We infer that in these
282 experiments, since the rising silicone was very close to the surface, the sagging of the sand overburden pushed
283 downward ~~the centre of~~ the silicone that, consequently, squeezed up at the edges of the cylinder. Such process may also
284 explain the two linear grabens that formed in the experiments with elliptical sources for small overburden thicknesses
285 (ratio $T/D \sim 0.1$, Brothelande and Merle 2015).

286 The deformation pattern observed in our experiments is independent of the imposed strain (i.e. uplift) rate or the
287 viscosity of the intruding material as suggested by the similarity with results obtained in previous studies with higher
288 strain rates (Acocella and Mulugeta, 2002) or lower viscosity intruding materials (Galletto et al., 2017; Marti et al. 1994;
289 Walter and Troll, 2001). On the other hand, the occurrence of an apical depression is dependent on the thickness (i.e.
290 depth) of the intrusion since thin intrusions relative to their depths will generate sub-circular domes without any apical
291 depression (Galland et al., 2009; Galland, 2012). Moreover, our results confirm that the apical depression width shows a
292 linear correlation with the source depth (Fig. 8) as estimated in Brothelande and Merle (2015) for elongated sources.
293 This evidence documents that such relation is independent of the source eccentricity or shape of the extensional
294 structures at the top of the dome (i.e. linear graben or sub-circular depression) suggesting that any elongation of the
295 surface structure represents only a minor complication of the basic deformation pattern as already pointed out by
296 (Roche et al., 2000).

297

298 5.2 Origin and extent of the resurgence in the LHVC

299 The distribution of alteration patterns and deformation characteristics of the post-caldera deposits can be used to infer
300 the origin and extent of the uplift within the Los Potreros resurgent caldera. In particular, we focus on the Holocene
301 Cuicuiltic Member, which blankets the caldera floor. ~~The extent of the local deformation and alteration of the ubiquitous~~
302 ~~7.4 ka Cuicuiltic Member, which blankets the caldera floor, allow constraining the spatio-temporal evolution of the~~
303 ~~surficial deformation and associated uplifts in Los Potreros.~~ Unaltered and undeformed deposits of the Cuicuiltic
304 Member crop out along the E-W Las Papas lineament and unconformably cover altered and faulted lavas and
305 ignimbrites along the Arroyo Grande and Maxtaloya scarps. Alteration and deformation of the Cuicuiltic Member occur
306 along the Los Humeros Fault scarp and within the apical depression of the Loma Blanca bulge. The vertical striations of
307 the trachyandesitic plug near the Los Humeros fault scarp suggest that the ascent of the plug induced the uplift, the
308 normal dip-slip faulting and alteration of the Cuicuiltic Member.

309 The observations suggest that Los Potreros is not a classic resurgent caldera (i.e. a caldera characterised by a large-scale
310 process localized in a single area) but is characterised by uplift pulses discontinuous in space and time, inducing small-
311 scale deformations at each pulse (Fig. 10a-d). In particular, it was active in the south and north-eastern sector of the
312 caldera, at Maxtaloya and Arroyo Grande (Fig. 10a), prior to the deposition of the Cuicuiltic Member (~ 7.4 ka), and
313 then shifted towards N along the Los Humeros and Loma Blanca scarps during and post the eruption of the Cuicuiltic
314 Member (Fig. 10b-d). The felsic lava found at the Los Humeros Fault scarp shows a similar mineral assemblage to the
315 felsic domes located further south (Fig. 4); thus, the Los Humeros scarp may represent the final stage (i.e. effusive

316 eruption of felsic magmas, (Fig. 10c) of the uplift process, which is thus driven by the ascent of relatively narrow
317 (hundreds of meters) and highly viscous felsic magma batches. This is supported by the N-S elongation of the identified
318 lava domes which is sub-parallel to the orientation of the measured fault planes (NNW-SSE), indicating that the
319 observed deformation is closely related to the post-caldera volcanism. The emplacement of such magma bodies is
320 inferred here to drive the recent uplift and deformation of the Loma Blanca bulge, as suggested by the active fumaroles
321 and extensive alteration of both the Cuicuiltic Member and post-caldera lavas (Fig. 10d). The recent emplacement of
322 shallow magma bodies should be considered as a possible scenario for the interpretation of the seismicity in Los
323 Potrerros, which have been so far interpreted as induced by geothermal exploitation (Lermo et al., 2018). In fact, the
324 highest magnitude of the recent seismicity reached between 3.2 and 4.2 and may well be consistent with a volcano-
325 tectonic origin due to shallow magma emplacement, more than induced by reinjection of hydrothermal fluids (cf. Evans
326 et al., 2012 and references therein).

327 To further support the above interpretation from field observations, results from the presented analogue models were
328 used to constrain the magma source depth from the geometrical parameters measured in the experiments (L_g , θ , α , Table
329 4). We calculated the theoretical overburden thickness (i.e. the intrusion depth, T_t , Table 4) as follow (Brothelande and
330 Merle, 2015):

$$331 \quad T_t = \frac{1}{2} L_g \times \frac{\sin(\theta + \alpha)}{\cos \theta} \quad (1)$$

332 Comparing the percentage difference (σ) between the imposed experimental (T) and theoretical (T_t) overburden
333 thickness values, we calculate the associated error in the evaluation of the intrusion depth in the models (σ , Table 4,
334 Fig.8). We then use equation (1) for the evaluation of the heat source depth at the Loma Blanca bulge considering $\sigma \sim$
335 40 % (maximum value of the experiments excluding those showing an annular depression that was not observed in the
336 field). For the Loma Blanca bulge $L_g = 286$ m, $\theta = 71^\circ$, $\alpha = 4.5^\circ$, the estimated intrusion depth is 425 ± 170 m. Such
337 relatively shallow depth is within the range of depths of rhyolitic-dacitic bodies drilled in geothermal wells (spanning
338 from -300 to -1700 m, Fig. 2a-b) and is consistent with the hypothesis that the uplift is driven by small and delocalized
339 magmatic intrusions, as suggested by the field data. These rhyolites-dacites bodies have been previously interpreted as
340 subaerial in origin (Carrasco-Núñez et al., 2017a), but we suggest that at least some of them can be reinterpreted as
341 intrusions of felsic cryptodomes based on the following considerations: (i) the occurrence of rhyolite-dacite lava bodies
342 within the thick pre-caldera old andesite sequence is unusual and does not have a subaerial counterpart; (ii) the rhyolite
343 body in well H-20 (Fig. 2b) up warps both the intracaldera ignimbrite sequence and the post-caldera lavas (showing a
344 reduced thickness) indicating that the caldera forming ignimbrites ~~do did not levelled~~ out the paleo-topography, ~~as it~~
345 ~~should be expected~~; and (iii) the top of the Xaltipan ignimbrite shows a higher depth variation than the pre caldera
346 andesite (Fig. 2a) highlighting a local and discontinuous uplifting of the Xaltipan ignimbrite. Such evidence can be
347 more easily reconciled with the intrusion of felsic cryptodomes within the volcanic sequence.

348

349 5.3 Implications for the structure of the LHVC geothermal field

350 The combination of field and modelling data support that the uplift in Los Potrerros caldera is due to multiple
351 deformation sources in narrow areas that do not represent resurgence *sensu stricto*. Such localized recent deformation
352 within Los Potrerros caldera appears to be linked to small magmatic intrusions located at relatively shallow depths (i.e. <
353 1 km) as in Loma Blanca, where the estimated intrusion depth calculated from the experimental data is 425 ± 170 m.

354 This model differs from the generally accepted idea of a resurgence in Los Potrerros induced by the inflation of a saucer
355 or cup shaped deep magmatic intrusion (Norini et al., 2015, 2019), which may be active at a larger scale but does not
356 explain the highly discontinuous deformation and alteration patterns with pulses scattered along the caldera floor.

357 ~~Neither~~ ~~Not even~~ the thermal anomalies identified by Norini et al. (2015) are compatible with the classic resurgence in
358 Los Potreros, since fit well with the classic resurgence as ground -temperatures are unexpectedly cold beneath the centre
359 of the inferred resurgent block, where the highest temperatures should be instead expected. By contrast, sharp and
360 narrow temperature peaks, spatially coincident with Los Humeros and Loma Blanca faults, are consistent with the
361 presence of shallow and delocalized heat sources. Indeed, the inflation of the deep magma chamber of the LHVC,
362 inferred to be at 5 to 7-8 km of depth (Verma, 1983, 2000, 2011) and extending 9 km in radius and 6 km in length (thus
363 coinciding with the Los Humeros caldera rim, Verma et al., 1990), should have induced a much wider uplift and with
364 higher magnitude than the one observed in the field. Resurgence resulting from magma remobilization of the deep
365 chamber that produced collapse is characterized by a larger-scale surface deformation (thousands of meters of uplift
366 extending for tens of kilometres on the surface) as shown in many large calderas worldwide (Toba, de Silva et al., 2015;
367 Cerro Galan, Folkes et al., 2011; Ischia, Carlino, 2012, Selva et al. 2019).

368 It is therefore unlikely that the replenishment of new magma in the caldera forming deep magma chamber accounts for
369 the magnitude (few tens of meters) and discontinuous spatial distribution of the deformation in Los Potreros.

370 Such a model of the recent uplifting in Los Potreros is supported by field-based petrographic-mineralogical analysis
371 showing that the present-day magmatic plumbing system is characterized by multiple magma levels spanning from a
372 deep (30-33 km) basaltic reservoir to very shallow (~ 1.5 km), smaller, trachyandesitic-trachytic magma batches (Lucci
373 et al., 2020).

374 A similar model of the plumbing system has been proposed to explain the eruptive activity of Usu volcano (Japan) since
375 1663, a post caldera cone of the Toya caldera consisting of a basaltic main edifice surmounted by three felsic lava
376 domes and more than ten cryptodomes. Petrochemical data at Usu suggest the presence of multiple magma batches (i.e.
377 sills) at 0.25-2 km deep that originated from partial melting of a metagabbro (Matsumoto and Nakagawa, 2010; Tomya
378 et al., 2010).

379 Our proposed model has implications for planning future geothermal exploration: siting of future geothermal wells
380 should consider that the presence of shallow heat sources within the caldera might complicate the pattern of isotherms
381 associated with the deeper heat flow.

382 **6 Conclusions**

383 By integrating field work with analogue models, we constrain the Late Pleistocene-Holocene spatio-temporal evolution
384 of volcanism of the LHVC and estimate the depth of the magmatic intrusions feeding the active geothermal system.
385 New findings on experimental analogue models of resurgent domes are also provided.

386 These are the main results that can be extracted from this study:

- 387 1. The distribution of the alteration patterns and deformation of the Cuicuiltic Member suggests that the recent (post-
388 caldera collapse) uplift in Los Potreros caldera moved progressively northwards, from the south and north-eastern
389 sector of the caldera towards N along the Los Humeros and Loma Blanca scarps.
- 390 2. The estimated depth of the intrusions responsible for such uplift is very shallow, as calculated from the experimental
391 data for the Loma Blanca bulge (425 ± 170 m).
- 392 3. The recent uplift in Los Potreros is discontinuous in space and time, inducing small-scale (areal extent ~ 1 km²)
393 deformations originating from multiple and shallow (< 1 km depth) magmatic bodies, thus not representing a classic
394 resurgent caldera, which usually involves large-scale deformation (areal extent of several km²).
- 395 4. The relationship between the depth of the magmatic source and the surface parameters of resurgent domes is
396 independent of the source eccentricity, ~~similarly to what already verified for sub-circular intrusions.~~

397

398 **Acknowledgements**

399 CFE is kindly acknowledged for allowing work on the Los Humeros geothermal field. Federico Galetto helped for laser
400 scanner data processing. Fabio Corbi and Matteo Trolese provided technical support in building the experimental set-up.
401 Gianluca Norini is acknowledged for logistic support in the field. Alessandra Pensa kindly helped with figure drawings.
402 Funded by the European Union's Horizon 2020 GEMex Project (grant agreement No. 727550) and by the Mexican
403 Energy Sustainability Fund CONACYT-SENER, WP 4.5 of the Project 2015-04-268074. More information can be
404 found on the GEMex Website: <http://www.gemex-h2020.eu>. The Grant to Department of Science, Roma Tre University
405 (MIUR-Italy Dipartimenti di Eccellenza, ARTICOLO 1, COMMI 314 – 337 LEGGE 232/2016) is gratefully
406 acknowledged.

407

408 **References**

- 409 Acocella, V.: Great challenges in volcanology: how does the volcano factory work?, *Front. Earth Sci.*, 2:4,
410 <https://doi.org/10.3389/feart.2014.00004>, 2014.
- 411 Acocella, V., and Funicello, R.: The interaction between regional and local tectonics during resurgent doming: the case
412 of the island of Ischia, Italy, *J. Volcanol. Geoth. Res.*, 88, 109-123, [https://doi.org/10.1016/S0377-0273\(98\)00109-7](https://doi.org/10.1016/S0377-0273(98)00109-7),
413 1999.
- 414 Acocella, V., and Mulugeta, G.: Experiments simulating surface deformation induced by pluton emplacement,
415 *Tectonophysics*, 352, 275-293, [https://doi.org/10.1016/S0040-1951\(02\)00218-4](https://doi.org/10.1016/S0040-1951(02)00218-4), 2002.
- 416 Acocella, V., Cifelli, F., and Funicello, R.: The control of overburden thickness on resurgent domes, *J. Volcanol. Geoth.*
417 *Res.*, 111, 137–153, [https://doi.org/10.1016/S0377-0273\(01\)00224-4](https://doi.org/10.1016/S0377-0273(01)00224-4), 2001.
- 418 Arellano, V.M., García, A., Barragán, R.M., Izquierdo, G., Aragón, A., and Nieva, D.: An updated conceptual model of
419 the Los Humeros geothermal reservoir (Mexico), *J. Volcanol. Geoth. Res.*, 124, 67–88, [https://doi.org/10.1016/S0377-0273\(03\)00045-3](https://doi.org/10.1016/S0377-0273(03)00045-3), 2003.
- 420
- 421 Beavon, R.V.: A resurgent cauldron in the early Paleozoic of Wales, U.K., *J. Volcanol. Geoth. Res.*, 7, 157-174,
422 [https://doi.org/10.1016/0377-0273\(80\)90025-6](https://doi.org/10.1016/0377-0273(80)90025-6), 1980.
- 423 Brothelande, E., Peltier, A., Got, J.L., Merle, O., Lardy, M., and Garaebiti, E.: Constraints on the source of resurgent
424 doming inferred from analogue and numerical modeling — Implications on the current feeding system of the Yenkahe
425 dome–Yasur volcano complex (Vanuatu), *J. Volcanol. Geoth. Res.*, 322, 225–240,
426 <https://doi.org/10.1016/j.jvolgeores.2015.11.023>, 2016.
- 427 Brothelande, E., and Merle, O.: Estimation of magma depth for resurgent domes: An experimental approach, *Earth*
428 *Planet. Sc. Lett.*, 412, 143–151, <https://doi.org/10.1016/j.epsl.2014.12.011>, 2015.
- 429 Calcagno, P., Evanno, G., Trumpy, E., Carlos Gutiérrez-Negrín, L., Macías, J.L., Carrasco-Núñez, G., and Liotta, D.:
430 Preliminary 3-D geological models of Los Humeros and Aocolulco geothermal fields (Mexico)-H2020 GEMex Project,
431 *Adv. Geosci.*, 45, 321–333, <https://doi.org/10.5194/adgeo-45-321-2018>, 2018.
- 432 Carlino, S.: The process of resurgence for Ischia Island (southern Italy) since 55 ka: The laccolith model and
433 implications for eruption forecasting, *B. Volcanol.*, 74, 947–961. <https://doi.org/10.1007/s00445-012-0578-0>, 2012.
- 434 Carrasco-Núñez, G., and Branney, M.J.: Progressive assembly of a massive layer of ignimbrite with a normal-to-reverse
435 compositional zoning: The Zaragoza ignimbrite of central Mexico, *B. Volcanol.*, 68, 3–20,
436 <https://doi.org/10.1007/s00445-005-0416-8>, 2005.

437 Carrasco-Núñez, G., McCurry, M., Branney, M.J., Norry, M., and Willcox, C.: Complex magma mixing, mingling, and
438 withdrawal associated with an intra-Plinian ignimbrite eruption at a large silicic caldera volcano: Los Humeros of
439 central Mexico, *Bull. Geol. Soc. Am.*, 124, 1793–1809, <https://doi.org/10.1130/B30501.1>, 2012.

440 Carrasco-Núñez, G., López-Martínez, M., Hernández, J., and Vargas, V.: Subsurface stratigraphy and its correlation
441 with the surficial geology at Los Humeros geothermal field, eastern Trans-Mexican Volcanic Belt, *Geothermics*, 67, 1–
442 17, <https://doi.org/10.1016/j.geothermics.2017.01.001>, 2017a.

443 Carrasco-Núñez, G., Hernández, J., De León, L., Dávila, P., Norini, G., Bernal, J.P., Jicha, B., Navarro, M., López-
444 Quiroz, P., and Digitalis, T.: Geologic Map of Los Humeros volcanic complex and geothermal field, eastern Trans-
445 Mexican Volcanic Belt, *Terra Digitalis*, 1, 1–11, <https://doi.org/10.22201/igg.terradigitalis.2017.2.24.78>, 2017b.

446 Carrasco-Núñez, G., Bernal, J.P., Dávila, P., Jicha, B., Giordano, G., and Hernández, J.: Reappraisal of Los Humeros
447 volcanic complex by new U/Th zircon and ⁴⁰Ar/³⁹Ar dating: Implications for greater geothermal potential, *Geochem.*
448 *Geophys. Geosy.*, 19, 132-149, <https://doi.org/10.1002/2017GC007044>, 2018.

449 Cashman, K. V., & Giordano, G.: Calderas and magma reservoirs, *J. Volcanol. Geoth. Res.*, 288, 28-45,
450 <https://doi.org/10.1016/j.jvolgeores.2014.09.007>, 2014.

451 Catalano, S., De Guidi, G., Lanzafame, G., Monaco, C., and Tortotici, L.: Late quaternary deformation on the island on
452 Pantelleria: new constraints for the recent tectonic evolution of the Sicily Channel Rift (southern Italy). *J. Geodyn.* 48,
453 75–82, 2009.

454 Chang, W.L., Smith, R.B., Wicks, C., Farrell, J.M., and Puskas, C.M.: Accelerated uplift and magmatic intrusion of the
455 Yellowstone Caldera, 2004 to 2006, *Science*, 318, 952-956, <https://doi.org/10.1126/science.1146842>, 2007.

456 Christiansen, R.L., Lipman, P.W., Carr, W.J., Byers, F.M., Orkild, P.P., and Sargent, K.A.: Timber Mountain-Oasis
457 Valley caldera complex of southern Nevada, *Geol. Soc. Am. Bull.*, 88, 943-959, [https://doi.org/10.1130/0016-7606\(1977\)88<943:TMVCCO>2.0.CO;2](https://doi.org/10.1130/0016-7606(1977)88<943:TMVCCO>2.0.CO;2), 1977.

459 Dávila-Harris, P., and Carrasco-Núñez, G.: An unusual syn-eruptive bimodal eruption: The Holocene Cuicuiltic
460 Member at Los Humeros caldera, Mexico, *J. Volcanol. Geoth. Res.*, 271, 24–42,
461 <https://doi.org/10.1016/j.jvolgeores.2013.11.020>, 2014.

462 de Silva, S.L., Mucek, A.E., Gregg, P.M., and Pratomo, I.: Resurgent Toba - field, chronologic, and model constraints
463 on time scales and mechanisms of resurgence at large calderas, *Front. Earth Sci.*, 3, 1–17,
464 <https://doi.org/10.3389/feart.2015.00025>, 2015.

465 Doblas, M.: Slickenside kinematic indicators, *Tectonophysics*, 295, 187–197, [https://doi.org/10.1016/S0040-1951\(98\)00120-6](https://doi.org/10.1016/S0040-1951(98)00120-6), 1998.

467 Du Bray, E.A., and Pallister, J.S.: Recrystallization and anatexis along the plutonic–volcanic contact of the Turkey
468 Creek caldera, Arizona, *Geol. Soc. Am. Bull.*, 111, 143–153, [https://doi.org/10.1130/0016-7606\(1999\)111<0143:RAAATP>2.3.CO;2](https://doi.org/10.1130/0016-7606(1999)111<0143:RAAATP>2.3.CO;2), 1999.

470 Elston, W.: Mid-Tertiary ash flow tuff cauldrons, southwestern New Mexico, *J. Geophys. Res.*, 89, 8733–8750,
471 <https://doi.org/10.1029/JB089iB10p08733>, 1984.

472 Evans, K.F., Zappone, A., Kraft, T., Deichmann, N., and Moia, F.: A survey of the induced seismic responses to fluid
473 injection in geothermal and CO₂ reservoirs in Europe, *Geothermics*, 41, 30-54,
474 <https://doi.org/10.1016/j.geothermics.2011.08.002>, 2012.

475 Ferrari, L., Orozco-Esquivel, T., Manea, V., and Manea, M.: The dynamic history of the Trans-Mexican Volcanic Belt
476 and the Mexico subduction zone, *Tectonophysics*, 522–523, 122–149, <https://doi.org/10.1016/j.tecto.2011.09.018>, 2012.

477 Ferriz, H., and Mahood, G.A.: Eruption Rates and Compositional Trends at Los Humeros Volcanic Center, Puebla,
478 Mexico, *J. Geophys. Res.*, 89, 8511-8524, <https://doi.org/10.1029/JB089iB10p08511>, 1984.

479 Folkes, C.B., Wright, H.M., R.A.F. Cas, de Silva, S.L., Lesti, C., and Viramonte, J.G.: A re-appraisal of the stratigraphy
480 and volcanology of the Cerro Galán volcanic system, NW Argentina, *B. Volcanol.*, 73, 1427–1454,
481 <https://doi.org/10.1007/s00445-011-0459-y>, 2011.

482 Fridrich, C.J., Smith, R.P., DeWitt, E., McKee, E.H.: Structural, eruptive, and intrusive evolution of the Grizzly Peak
483 caldera, Sawatch Range, Colorado, *Geol. Soc. Am. Bull.*, 103, 1160-1177, [https://doi.org/10.1130/0016-7606\(1991\)103<1160:SEAIEO>2.3.CO;2](https://doi.org/10.1130/0016-7606(1991)103<1160:SEAIEO>2.3.CO;2), 1991.

485 Galetto, F., Acocella, V., and Caricchi, L.: Caldera resurgence driven by magma viscosity contrasts, *Nat. Commun.*, 8,
486 1–11, <https://doi.org/10.1038/s41467-017-01632-y>, 2017.

487 Galetto, F., Bagnardi, M., Acocella, V., and Hooper, A.: Noneruptive unrest at the caldera of Alcedo Volcano (Galápagos
488 Islands) revealed by InSAR data and geodetic modelling, *J. Geophys. Res.*, 124, 3365–3381,
489 <https://doi.org/10.1029/2018JB017103>, 2019.

490 Galland, O.: Experimental modelling of ground deformation associated with shallow magma intrusions, *Earth Planet.
491 Sc. Lett.*, 317-318, 145-156, <https://doi.org/10.1016/j.epsl.2011.10.017>, 2012.

492 Galland, O., Planke, S., Ragnhild Neumann, E., and Malthe-Sørenssen, A.: Experimental modelling of shallow magma
493 emplacement: Application to saucer-shaped intrusions, *Earth Planet. Sc. Lett.*, 277, 373-383,
494 <https://doi.org/10.1016/j.epsl.2008.11.003>, 2009.

495 Giordano, G., Pinton, A., Cianfarra, P., Baez, W., Chiodi, A., Viramonte, J., Norini G., and Groppelli, G.: Structural
496 control on geothermal circulation in the Cerro Tuzgle–Tocomar geothermal volcanic area (Puna plateau, Argentina), *J.
497 Volcanol. Geotherm. Res.*, 249, 77-94. <https://doi.org/10.1016/j.jvolgeores.2012.09.009>, 2013

498 Giordano, G., De Benedetti, A. A., Bonamico, A., Ramazzotti, P., and Mattei, M.: Incorporating surface indicators of
499 reservoir permeability into reservoir volume calculations: Application to the Colli Albani caldera and the Central Italy
500 Geothermal Province, *Earth-Sci. Rev.*, 128, 75-92, <https://doi.org/10.1016/j.earscirev.2013.10.010>, 2014.

501 Goto, Y., and McPhie, J.: Tectonics, structure, and resurgence of the largest Quaternary caldera in Japan: Kutcharo,
502 Hokkaido, *Geol. Soc. Am. Bull.*, 130, 1307-1322, <https://doi.org/10.1130/B31900.1>, 2018.

503 Guillou-Frottier, L., Burov, E.B., and Milési, J.P.: Genetic links between ash-flow calderas and associated ore deposits
504 as revealed by large-scale thermo-mechanical modelling, *J. Volcanol. Geoth. Res.*, 102, 339–361,
505 [https://doi.org/10.1016/S0377-0273\(00\)00246-8](https://doi.org/10.1016/S0377-0273(00)00246-8), 2000.

506 Hildreth, W., Fierstein, J., and Calvert, A.: Early postcaldera rhyolite and structural resurgence at Long Valley
507 Caldera, California, *J. Volcanol. Geoth. Res.*, 335, 1-34, <http://dx.doi.org/10.1016/j.jvolgeores.2017.01.005>, 2017.

508 Kennedy, B., Wilcock, J., and Stix, J.: Caldera resurgence during magma replenishment and rejuvenation at Valles and
509 Lake City calderas, *B. Volcanol.*, 74, 1833–1847, <https://doi.org/10.1007/s00445-012-0641-x>, 2012.

510 [Kennedy, B., Holohan, E.P., Stix, J., Gravelly, D.M., Davidson, J.R.J., and Cole, J.W.: Magma plumbing beneath](https://doi.org/10.1016/j.earscirev.2017.12.002)
511 [collapse caldera volcanic systems, *Earth-Sci. Rev.*, 177, 404–424, https://doi.org/10.1016/j.earscirev.2017.12.002, 2018.](https://doi.org/10.1016/j.earscirev.2017.12.002)

512

513 Lipman, P. W.: The roots of ash flow calderas in Western North America: windows into the tops of granitic batholiths, *J.
514 Geophys. Res.*, 89, 8801–8841, <https://doi.org/10.1029/JB089iB10p08801>, 1984.

515 Lermo, J., Lorenzo, C., Jiménez, N., Ramos, E., Ángulo, J., Israel, J., Téllez, N., Machado, O., Álvarez, I., Torres, R.,
516 Alfaro R.: Análisis de la actividad sísmica (1994-2016), su relación con los pozos inyectoros y productores y aplicación

517 de nuevas técnicas geofísica para caracterizar las zonas anómalas del campo geotérmico de Los Humeros, CEMIE-
518 GEO, Mexico, Internal Rep., 42 pp., 2018.

519 Lucci, F., Carrasco-Núñez, G., Rossetti, F., Theye, T., White, J. C., Urbani, S., Azizi, H., Asahara, Y., and Giordano, G.:
520 Anatomy of the magmatic plumbing system of Los Humeros Caldera (Mexico): implications for geothermal systems,
521 *Solid Earth Discuss.*, <https://doi.org/10.5194/se-2019-86>, 2020.

522 Marsh, B.D.: On the mechanics of caldera resurgence, *J. Geophys. Res.*, 89, 8245–8251,
523 <https://doi.org/10.1029/JB089iB10p08245>, 1984.

524 Martí, J., Ablay, G.J., Redshaw, L.T., and Sparks, R.S.J.: Experimental studies of collapse calderas, *J. Geol. Soc.*
525 *London*, 151, 919–929, <https://doi.org/10.1144/gsjgs.151.6.0919>, 1994.

526 Merle, O., Borgia, A.: Scaled experiments of volcanic spreading, *J. Geophys. Res.*, 101, 13805–13817,
527 <https://doi.org/10.1029/95JB03736>, 1996.

528 Morán-Zenteno, D.J., Alba-Aldave, L.A., Solé, J., and Iriondo, A.: A major resurgent caldera in southern Mexico: the
529 source of the late Eocene Tilzapotla ignimbrite. *J. Volcanol. Geoth. Res.*, 136, 97–119,
530 <https://doi.org/10.1016/j.jvolgeores.2004.04.002>, 2004.

531 Moretti, R., Troise, C., Sarno, F., and De Natale, G.: Caldera unrest driven by CO₂ induced drying of the deep
532 hydrothermal system, *Sci. Rep. UK*, 8, <https://doi.org/10.1038/s41598-018-26610-2>, 2018.

533 Mueller, W.U., Stix, J., Corcoran, P.L., Daigneault, R.: Subaqueous calderas in the Archean Abitibi greenstone belt: An
534 overview and new ideas, *Ore Geol. Rev.*, 35, 4–46, <https://doi.org/10.1016/j.oregeorev.2008.12.003>, 2009.

535 Norini, G., Groppelli, G., Sulpizio, R., Carrasco-Núñez, G., Dávila-Harris, P., Pelliccioli, C., Zucca, F., and De Franco,
536 R.: Structural analysis and thermal remote sensing of the Los Humeros Volcanic Complex: Implications for volcano
537 structure and geothermal exploration, *J. Volcanol. Geoth. Res.*, 301, 221–237,
538 <https://doi.org/10.1016/j.jvolgeores.2015.05.014>, 2015.

539 Norini, G., Carrasco-Núñez, G., Corbo-Camargo, F., Lermo, J., Hernández Rojas, J., Castro, C., Bonini, M., Montanari,
540 D., Corti, G., Moratti, G., Chavez, G., Ramirez, M., and Cedillo F.: The structural architecture of the Los Humeros
541 volcanic complex and geothermal field, *J. Volcanol. Geoth. Res.*, 381, 312–329.
542 <https://doi.org/10.1016/j.jvolgeores.2019.06.010>, 2019.

543 Matsumoto, A., and Nakagawa, M.: Formation and evolution of silicic magma plumbing system: Petrology of the
544 volcanic rocks of Usu volcano, Hokkaido, Japan, *J. Volcanol. Geoth. Res.*, 196, 185–207,
545 <https://doi.org/10.1016/j.jvolgeores.2010.07.014>, 2010.

546 Pribnow, D.F.C., Schütze, C., Hurter, S.J., Flechsig, C., Sass, J.H.: Fluid flow in the resurgent dome of Long Valley
547 Caldera: Implications from thermal data and deep electrical sounding. *J. Volcanol. Geoth. Res.*, 127, 329–345,
548 [https://doi.org/10.1016/S0377-0273\(03\)00175-6](https://doi.org/10.1016/S0377-0273(03)00175-6), 2003.

549 Roche, O., Druitt, T.H., and Merle, O.: Experimental study of caldera formation, *J. Geophys. Res.*, 105,
550 <https://doi.org/10.1029/1999JB900298>, 395–416, 2000.

551 Selva, J., Acocella, V., Bisson, M., Caliro, S., Costa, A., Della Seta, M., P. De Martino, S. de Vita, C. Federico,
552 G. Giordano, S. Martino, and C. Cardaci.: Multiple natural hazards at volcanic islands: a review for the Ischia volcano
553 (Italy), *Journal of Applied Volcanology*, 8(1), 5., <https://doi.org/10.1186/s13617-019-0086-4>, 2019

554 Smith, R. L., and Bailey, R. A.: Resurgent cauldrons, *Geol. Soc. Am. Mem.*, 116, 613–662,
555 <https://doi.org/10.1130/MEM116>, 1968.

556 Stix, J., Kennedy, B., Hannington, M., Gibson, H., Fiske, R., Mueller, W., Franklin, J.: Caldera-forming processes and
557 the origin of submarine volcanogenic massive sulfide deposits, *Geology*, 31, 375–378, [https://doi.org/10.1130/0091-
558 7613\(2003\)031<0375:CFPATO>2.0.CO;2](https://doi.org/10.1130/0091-7613(2003)031<0375:CFPATO>2.0.CO;2), 2003.

559 Swanson, E., and McDowell, F.: Geology and geochronology of the Tomochic caldera, Chihuahua, Mexico, *Geol. Soc.
560 Am. Bull.*, 96, 1477-1482, [https://doi.org/10.1130/0016-7606\(1985\)96<1477:GAGOTT>2.0.CO;2](https://doi.org/10.1130/0016-7606(1985)96<1477:GAGOTT>2.0.CO;2), 1985.

561 Tomiya, A., Takahashi, E., Furukawa, N., Suzuki, T.: Depth and evolution of a silicic magma chamber: Melting
562 experiments on a low-K rhyolite from Usu volcano, Japan, *J. Petrol.*, 51, 1333–1354,
563 <https://doi.org/10.1093/petrology/egq021>, 2010.

564 Ueda, H., Nagai, M., and Tanada, T.: Phreatic eruptions and deformation of Ioto Island (Iwo-jima), Japan, triggered by
565 deep magma injection, *Earth Planets Space*, 70, <https://doi.org/10.1186/s40623-018-0811-y>, 2018.

566 Verma, M.P., Verma, S.P., and Sanvicente, H.: Temperature field simulation with stratification model of magma
567 chamber under Los Humeros caldera, Puebla, Mexico, *Geothermics*, 19, 187–197, [https://doi.org/10.1016/0375-
568 6505\(90\)90015-4](https://doi.org/10.1016/0375-6505(90)90015-4), 1990.

569 Verma, S.P., Gómez-Arias, E., and Andaverde, J.: Thermal sensitivity analysis of emplacement of the magma chamber
570 in Los Humeros caldera, Puebla, Mexico, *Int. Geol. Rev.*, 53, 905–925, <https://doi.org/10.1080/00206810903234296>,
571 2011.

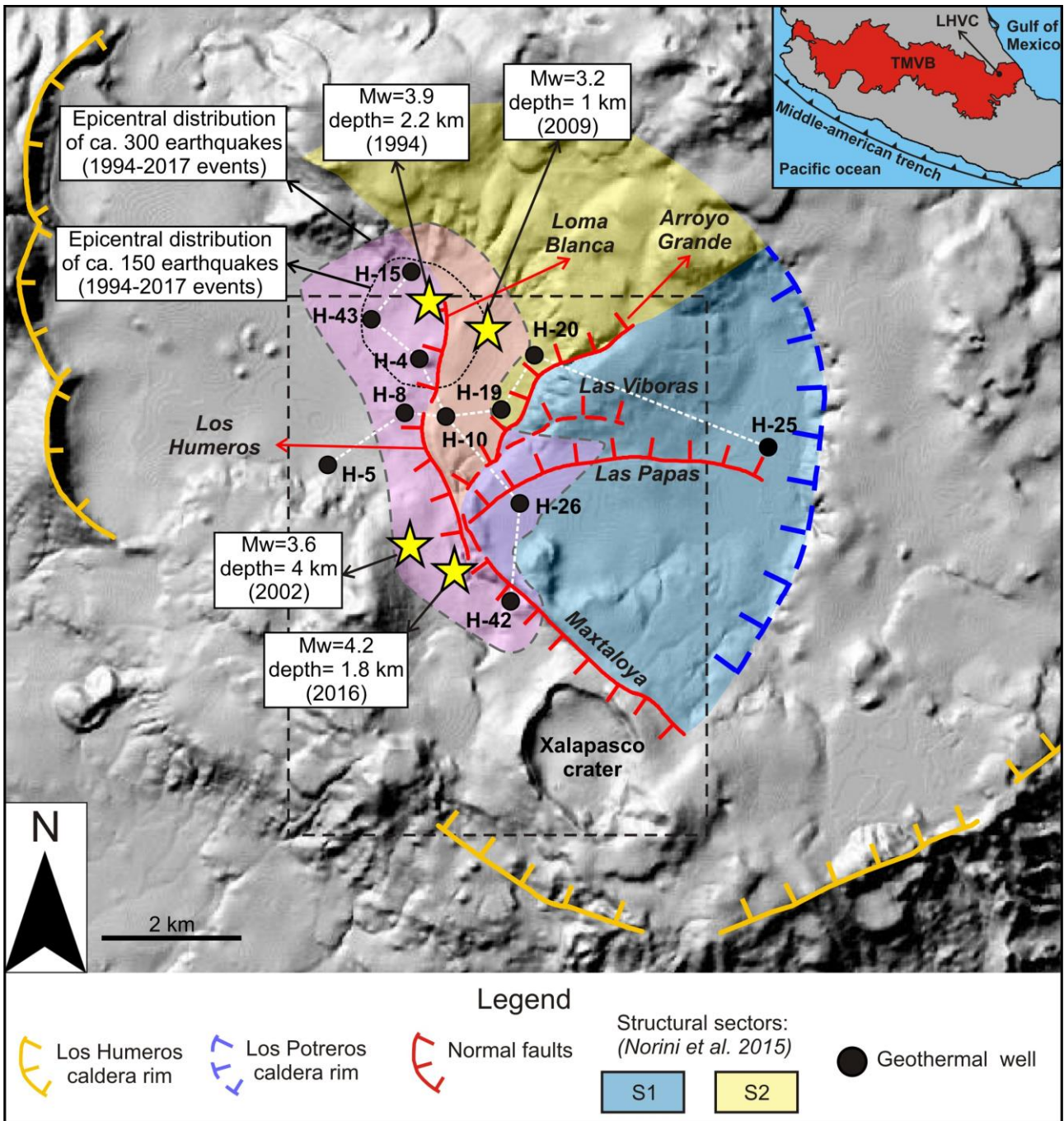
572 Verma, S.P.: Magma genesis and chamber processes at Los Humeros caldera, Mexico - Nd and Sr isotope data, *Nature*,
573 302, 52–55, <https://doi.org/10.1038/302052a0>, 1983.

574 Verma, S.P.: Geochemical evidence for a lithospheric source for magmas from Los Humeros caldera, Puebla, Mexico.
575 *Chem. Geol.* 164, 35–60, [https://doi.org/10.1016/S0009-2541\(99\)00138-2](https://doi.org/10.1016/S0009-2541(99)00138-2), 2000.

576 Vignaroli, G., Pinton, A., De Benedetti, A. A., Giordano, G., Rossetti, F., Soligo, M., and Berardi, G.: Structural
577 compartmentalisation of a geothermal system, the Torre Alfina field (central Italy), *Tectonophysics*, 608, 482-498.
578 <https://doi.org/10.1016/j.tecto.2013.08.040>, 2013. Vignaroli, G., Aldega, L., Balsamo, F., Billi, A., De Benedetti, A. A.,
579 De Filippis, L., Giordano G. and Rossetti, F.: A way to hydrothermal paroxysm, Colli Albani volcano, Italy, *Geol. Soc.
580 Am. Bull.*, 127(5-6), 672-687. <https://doi.org/10.1130/B31139.1>, 2015.

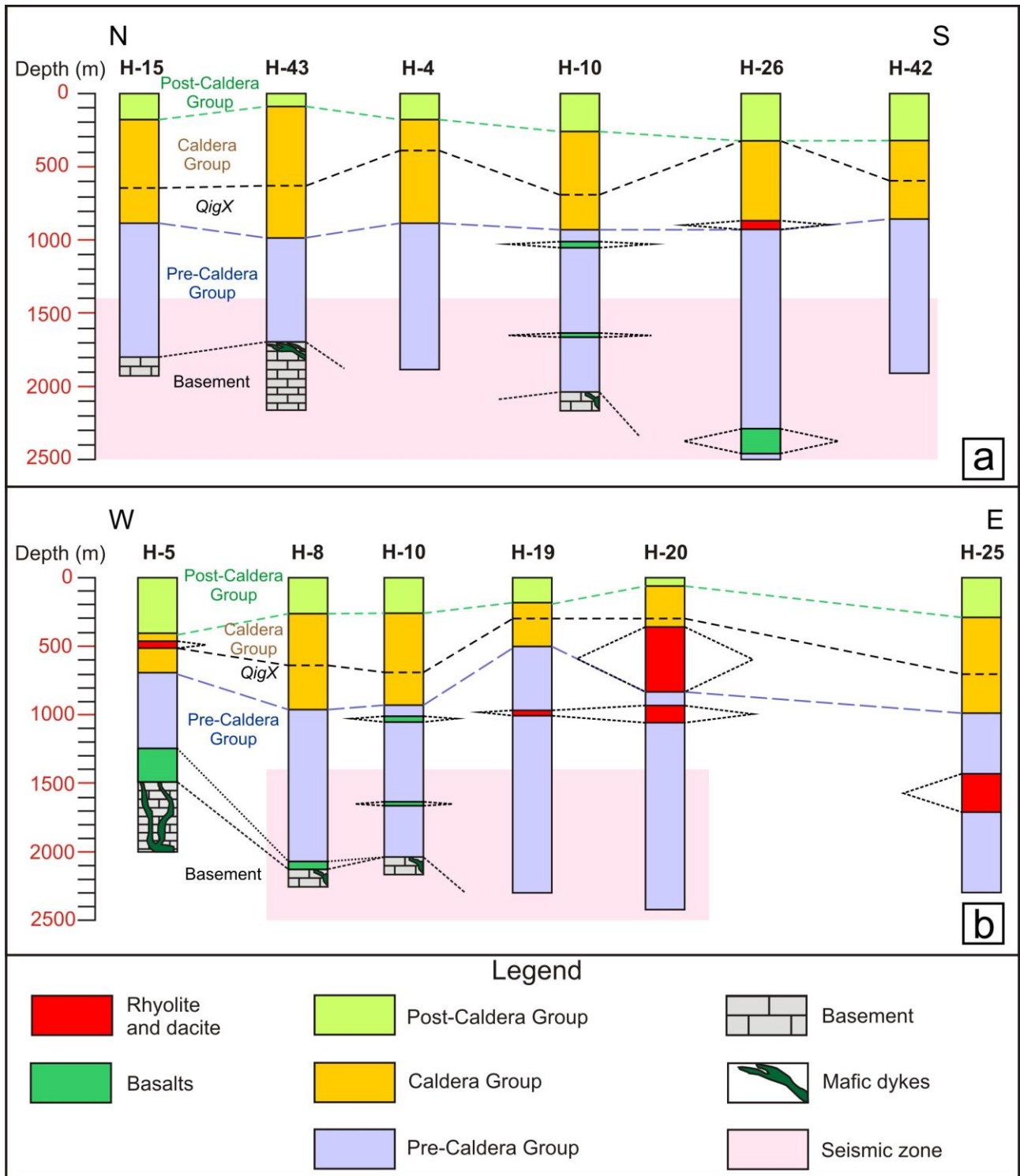
581 Walter, T.R., and Troll, V.R.: Formation of caldera periphery faults: an experimental study, *B. Volcanol.*, 63, 191-203,
582 <https://doi.org/10.1007/s004450100135>, 2001. Walter, T.R., Wang, R., Acocella, V., Neri, M., Grosser, H., and Zschau, J:
583 Simultaneous magma and gas eruptions at three volcanoes in southern Italy: an earthquake trigger ?, *Geology*, 37, 251–
584 254, <https://doi.org/10.1130/G25396A>, 2009.

585 Wilcox, C.P.: Eruptive, magmatic and structural evolution of a large explosive caldera volcano, Los Humeros, Central
586 Mexico, Ph.D. thesis, Department of Geology, University of Leicester, United Kingdom, 317 pp., 2011.



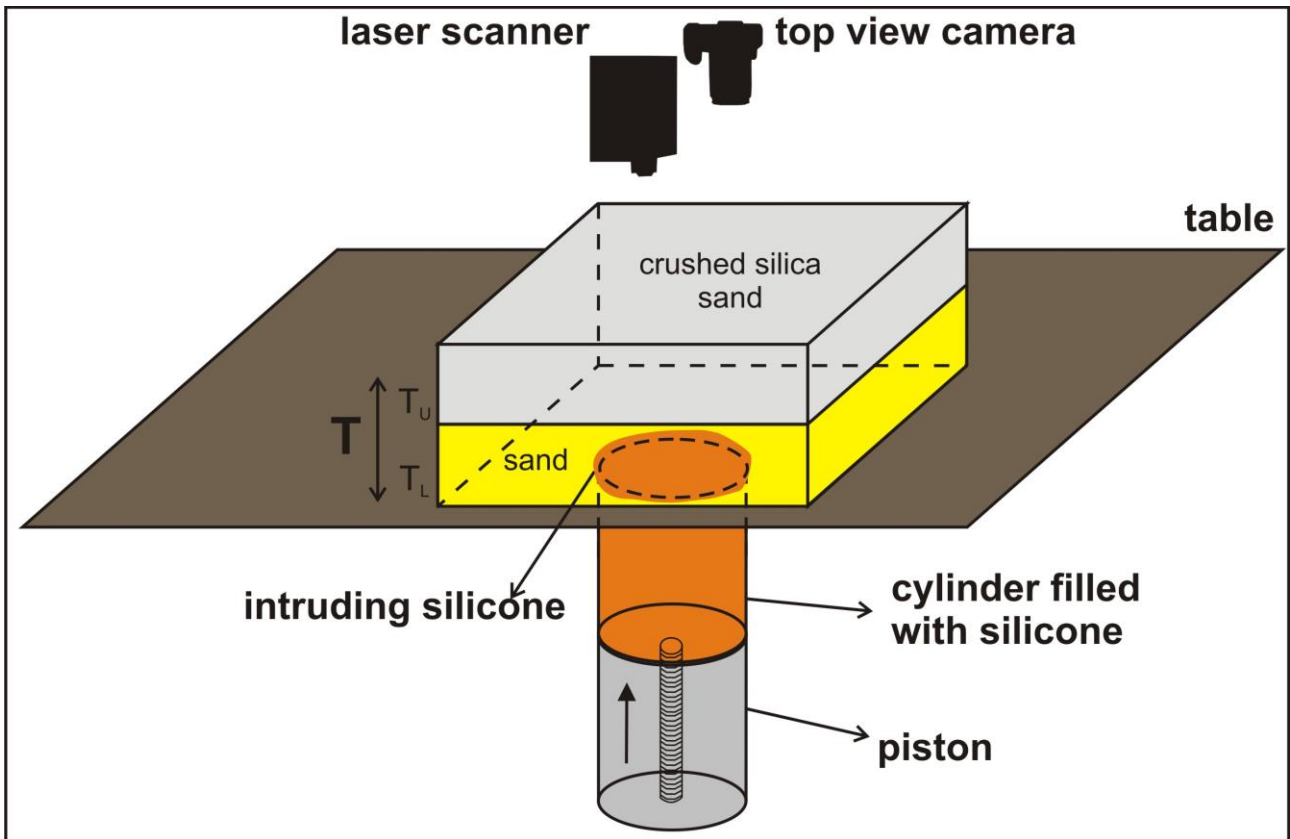
587
 588 **Figure 1:** Shaded relief image (illuminated from the NE) obtained from 15 m resolution DEM of the Los Humeros Volcanic
 589 Complex (LHVC) showing the main structural features (faults and caldera rim, modified from Norini et al. (2015); Calcagno
 590 et al. (2018) and some geothermal wells referred in the text and in Figures 2a-b. The white dashed lines indicate the direction
 591 of the correlation sections shown in Figures 2a-b. The black rectangle indicates the studied area within the Los Potreros
 592 Caldera shown in Figure 4. The Inset box show the location of the LHVC (black dot and arrow) within the eastern sector of
 593 the Trans Mexican Volcanic Belt (TMVB). The structural sectors S1 and S2 correspond to the resurgent block inferred by
 594 Norini et al. (2015). Seismicity data from Lermo et al. (2018).

595
 596
 597
 598
 599



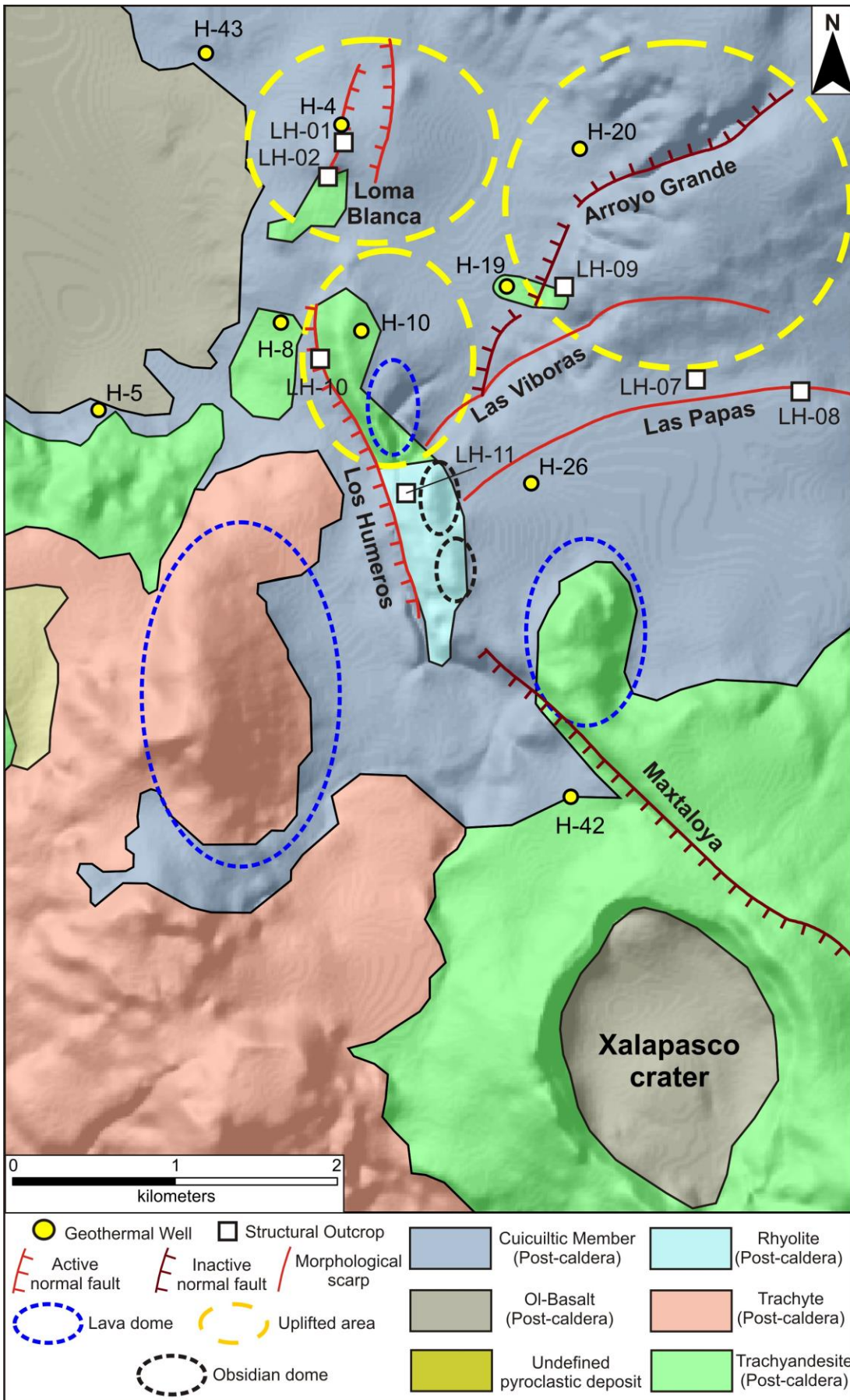
600
601
602
603

Figure 2: In depth correlation of lithostratigraphic units along the N-S (a) and W-E (b) direction (redrawn after Carrasco-Núñez et al. (2017a) and Arellano et al. (2003). Depth:horizontal distance=1:1. Location of the correlation line is shown in Figure 1. QigX= Xaltipan ignimbrite.



604
 605
 606
 607
 608
 609
 610
 611
 612
 613
 614
 615
 616
 617
 618
 619
 620
 621
 622
 623
 624
 625
 626
 627

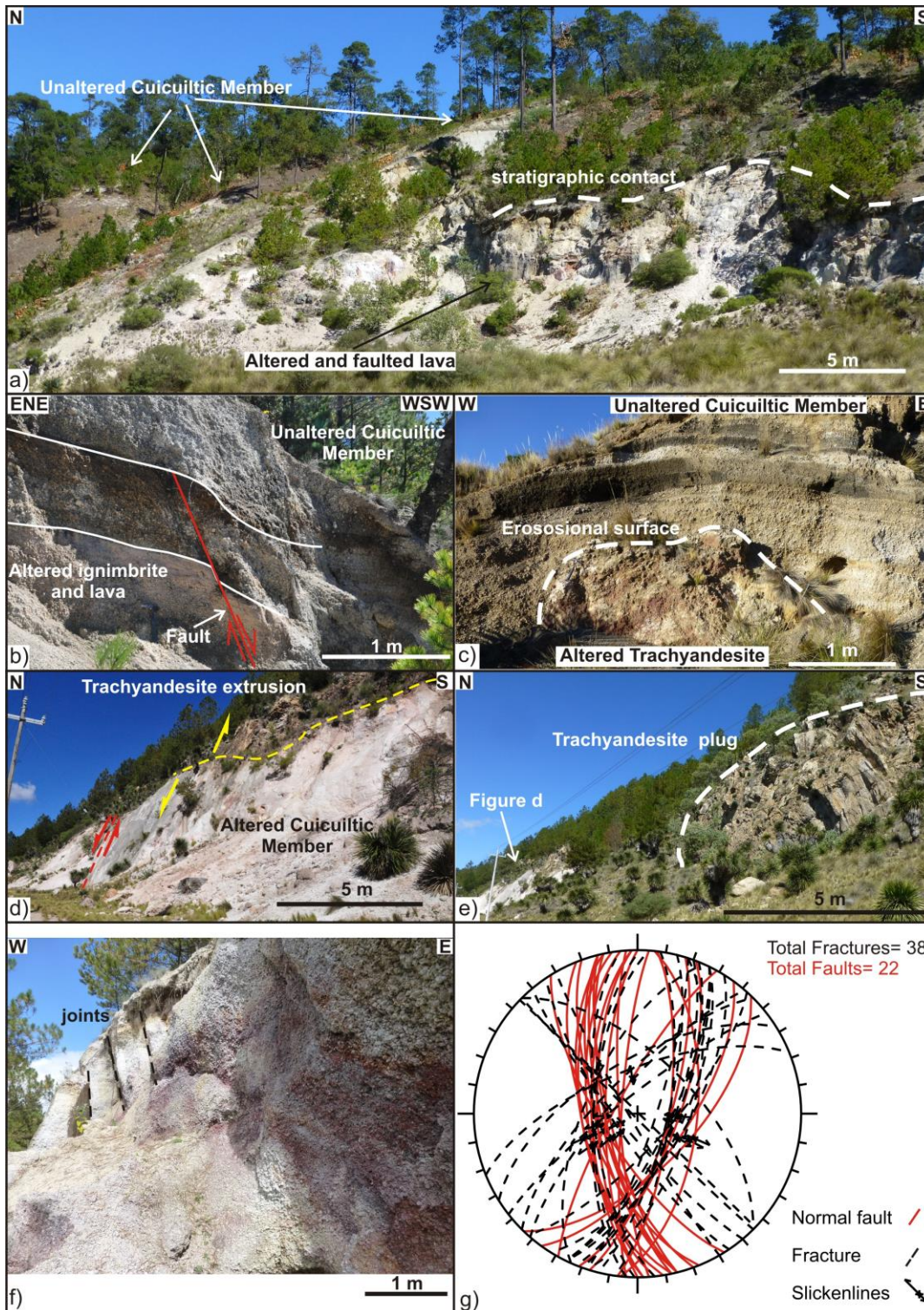
Figure 3: Experimental set-up. A motor controlled piston pushes upward the silicone at a fixed rate (2mm/hr) from the base of the layered sand pack (the diameter of the silicone is 8 cm). A laser scanner and a camera record the surface deformation induced by the intruding silicone. T = total overburden thickness. T_U = upper layer thickness, T_L = lower layer thickness.



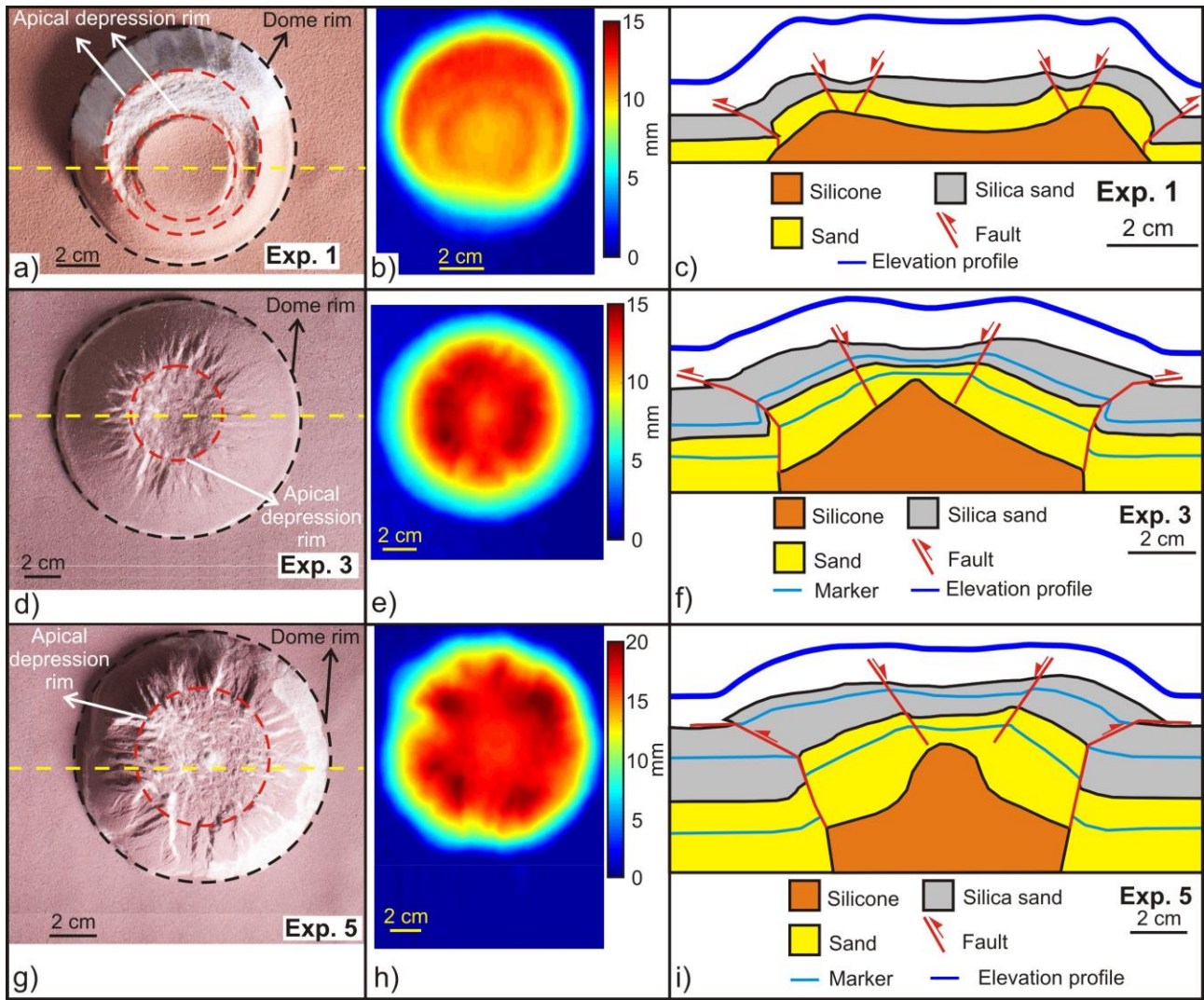
628
629 **Figure 4: Simplified geological structural map of the studied area;reinterpreted after (Norini et al., 2015; Carrasco- Núñez et**
630 **al., 2017b; Calcagno et al., 2018).**



631
 632 **Figure 5: a) Panoramic view from Xalapasco crater (looking towards N) of the lava domes aligned N-S. b) Unaltered**
 633 **Cuicuiltic Member (LH-07). c) Unaltered Cuicuiltic Member covering a layered pyroclastic deposit, which can be laterally**
 634 **correlated with the Xoxoctic Tuff (LH-08). The erosional surface preceding the deposition of the Cuicuiltic Member is shown**
 635 **(dashed white line).**

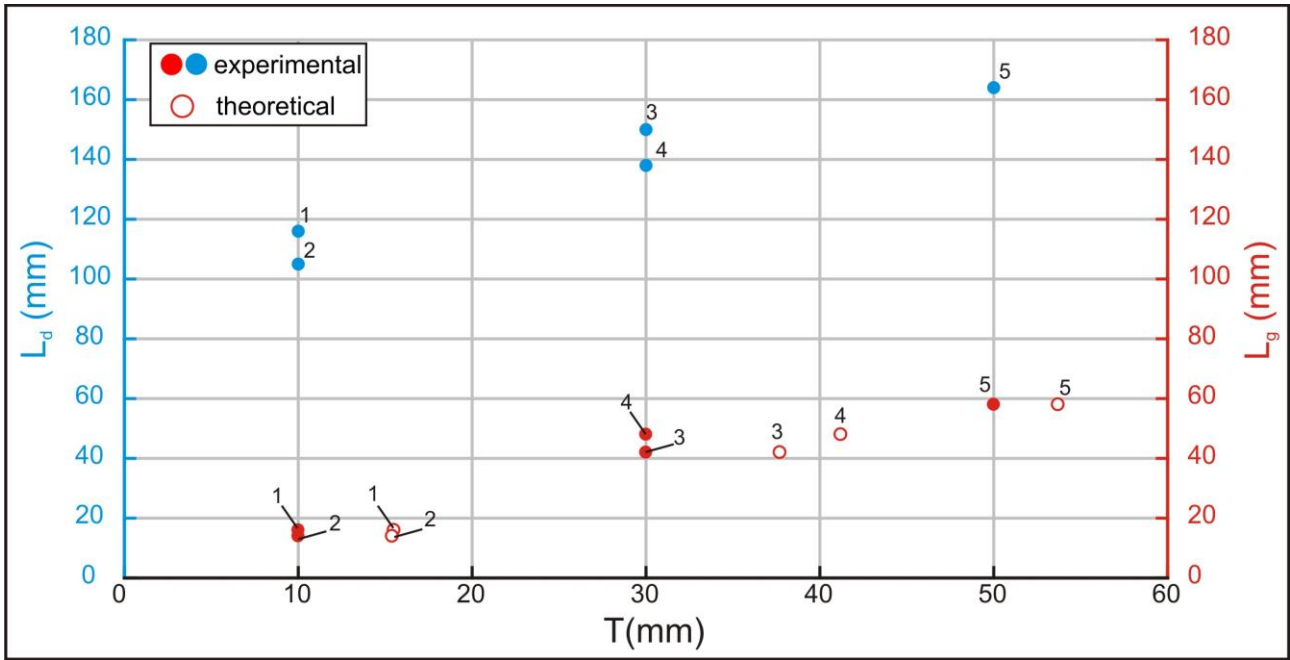


636
 637 **Figure 6:** a) Panoramic view of the Arroyo Grande fault scarp showing the unaltered Cuicuiltic Member covering the altered
 638 and faulted ignimbrite and lavas (site LH-09). b) Normal fault affecting the altered ignimbrite deposits unconformably
 639 covered by the post-caldera, unaltered Cuicuiltic Member deposits (LH-09). Note that the Cuicuiltic Member deposits are
 640 not faulted at this location; the fault can be thus considered as a fossil fault with respect to the Cuicuiltic Member deposition.
 641 c) Block of altered trachyandesite buried by unaltered Cuicuiltic Member layers along the Maxtaloya fault scarp. d) Los
 642 Humeros fault scarp (LH-10) induced by the ascent of the trachyandesitic extrusion on top of the fault plane. e)
 643 Trachyandesite plug cropping out ~150 southward the fault scarp shown in d) (indicated by the red arrow). f) Jointing and
 644 alteration of the Cuicuiltic Member within the apical depression of the Loma Blanca dome (LH-01). e) Equal-area stereo-plot
 645 of the attitudes of faults and fractures in all the structural outcrops.



646
647
648
649
650
651
652
653
654
655
656
657
658
659
660
661
662
663
664

Figure 7: a) d) g) Top view image of the experiments 1, 3 and 5. b) e) h) cumulative vertical displacement; colour scale is proportional to the amount of uplift. c) f) i) Drawing of the cross section view obtained after cutting the section close to the dome center. The elevation profiles are obtained from laser scanner data. The yellow dashed line in a) d) g) indicates the trace of the section views and of the elevation profiles.

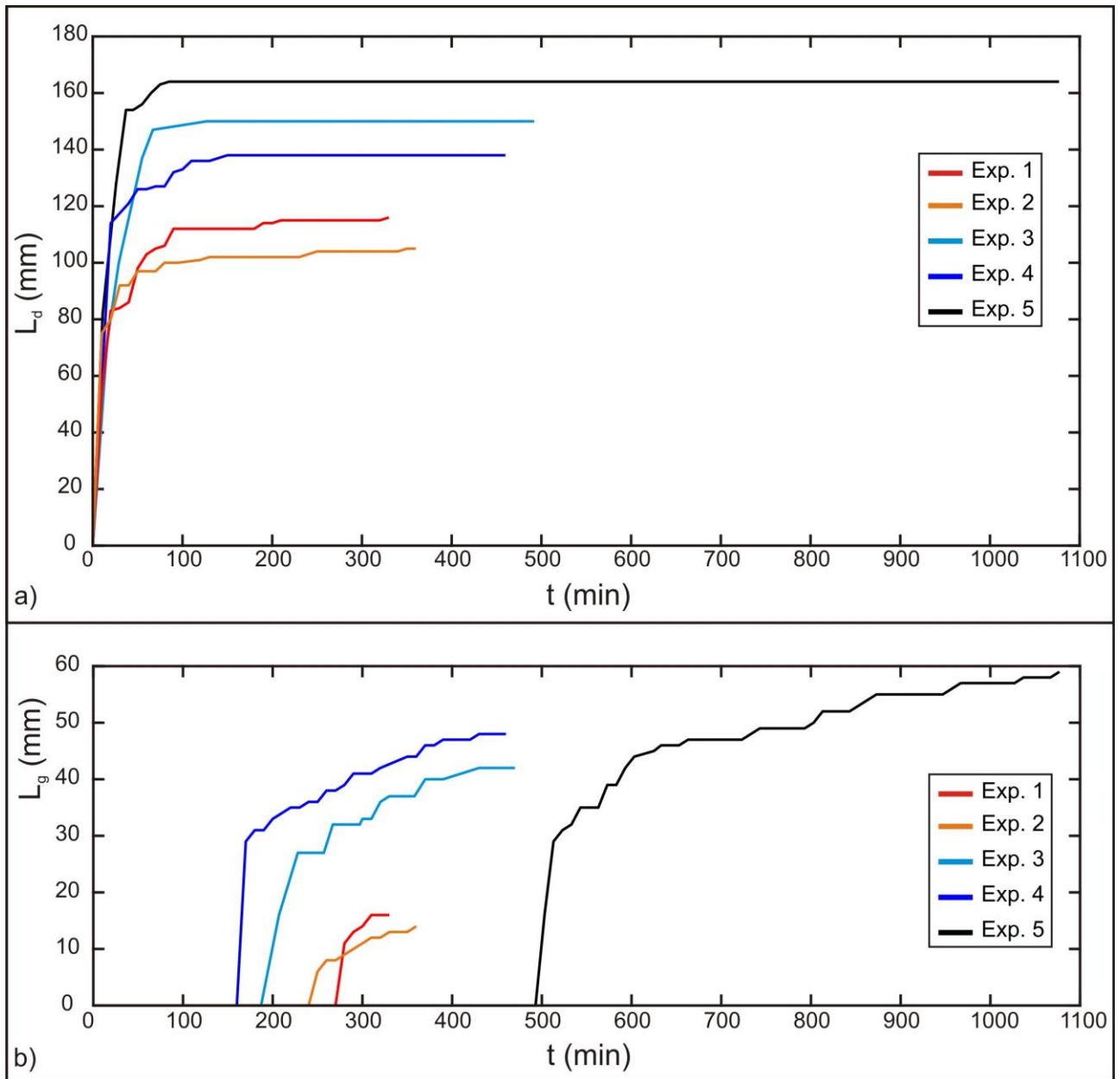


665

666

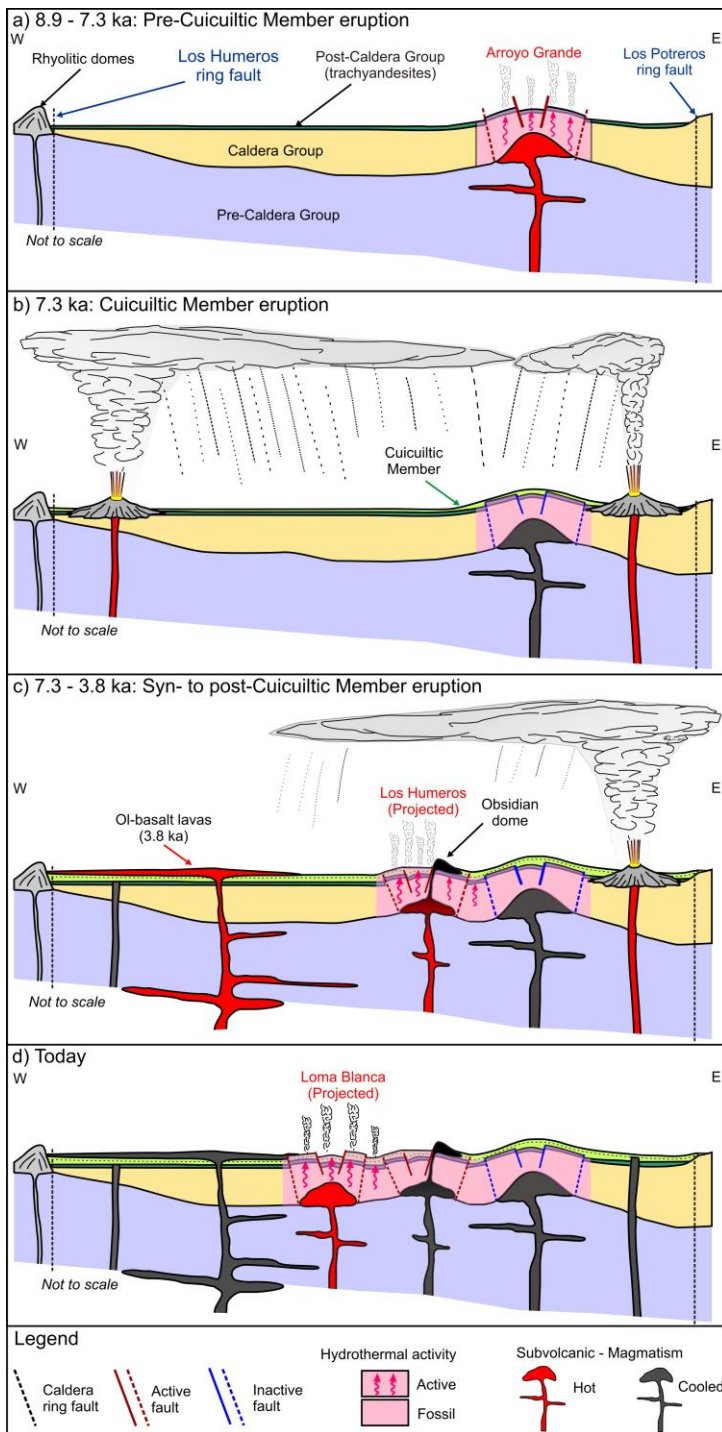
667

Figure 8: L_g (apical depression width) and L_d (dome diameter) versus T (overburden thickness). Theoretical values calculated after equation 1 (see discussion section). The numbers above each point indicate the experiment number.



668
 669 **Figure 9: a) Time evolution of the dome diameter (L_d). b) Time evolution of the apical depression width (L_g). Both L_d and L_g**
 670 **show a similar evolution trend with a first stage of abrupt increase at the beginning of each experiment. In the second stage**
 671 **L_d becomes constant at $t \sim 90$ min (experiments 1-2-3), $t \sim 150$ min (experiment 4) and $t \sim 65$ min (experiment 5) while L_g**
 672 **increases slightly from $t \sim 250$ -280 min (experiments 1-2), $t \sim 210$ min and ~ 170 min (experiments 3 and 4) and $t \sim 530$ min**
 673 **(experiment 5) till the end of the experiment.**

674
 675
 676
 677
 678
 679
 680
 681
 682
 683



684

685

686

687

688

689

690

691

692

693

694

695

Figure 10: Schematic model of the evolution of the sub-surface structure of the Los Potreros caldera floor. Multiple magmatic intrusions located at relatively shallow depth (< 1 km) are responsible for the localized bulging of the caldera floor (Loma Blanca, Los Humeros and Arroyo Grande uplifted areas). a) Pre Cuicuiltic Member eruption: emplacement of a felsic intrusion at shallow depth and formation of the Arroyo grande bulge characterized by extensional faulting at its top, reverse faulting at its base and hydrothermalism. b) Cuicuiltic Member eruption: eruption of the Cuicuiltic Member covering the hydrothermally altered post-caldera trachyandesitic lavas. c) Syn to post Cuicuiltic Member eruption: formation of the Los Humeros fault and extrusion of obsidian lava domes along the fault scarp. As the trachyandesitic domes are covered with Cuicuiltic Member only at his base, the lava extrusion occurred during and post the Cuicuiltic Member eruption. d) Formation of the Loma Blanca bulge with the current hydrothermal activity and extensional faulting occurring within the apical depression. Notice that the emplacement of the successive most recent domes (Los Humeros and Loma blanca) are not aligned on the same plane, they are shown for practical purposes.

Stage	Age (ka)	Main stratigraphic units
Post-caldera	< 69	Cuicuiltic Member and trachyandesitic to basaltic lavas
		Llano Tuff
		Xoxoctic Tuff
		Rhyolitic domes
Caldera	164-69	Zaragoza ignimbrite
		Faby Tuff
		Xaltipan ignimbrite
Pre-Caldera	700-164	Rhyolitic Domes

696 Table 1 Summary of the main stratigraphic units of the three evolutionary stages of the Los Humeros Volcanic complex
697 (Carrasco-Núñez et al., 2017b, 2018).

Parameter	Definition	Value (experiments)	Value (nature)
T	Thickness of the overburden	1-5 X 10 ⁻² m	300-2000 m
L _d	Dome diameter	1-1.6 X 10 ⁻¹ m	2000 m
H	Dome height	1.1-2 X 10 ⁻² m	100 m
ρ _s	Density of brittle overburden	1400 kg/m ³	2800 kg/m ³
φ	Angle of internal friction	35°	25-40°
τ ₀	Cohesion (brittle overburden)	300 Pa	10 ⁶ Pa
ρ _m	Density of intrusive material	1000 kg/m ³	2500 kg/m ³
μ _m	Viscosity of intrusive material	10 ⁴ Pa s	10 ¹⁵ Pa s
g	Gravity	9.8 m/s ²	9.8 m/s ²
t	Timespan for deformation	2.8-6.5 X 10 ⁴ s	1.9 X 10 ¹² s

698 Table 2. Comparison of the geometric and material properties parameters of the experiments and nature.

Dimensionless ratio	Experiments	Nature
Π ₁ = T/L _d	0.1-0.5	0.15-1
Π ₂ = H/L _d	0.08-0.2	0.05-0.1
Π ₃ = ρ _s /ρ _m	1.4	1.12
Π ₄ = φ	35	25-40
Π ₅ = ρ _m H ² /μ _{mt}	6.1 X 10 ⁻¹⁰	1.3 X 10 ⁻²⁰
Π ₆ = ρ _m gHt/μ _m	1.3 X 10 ³	4.6 X 10 ³
Π ₇ = ρ _s gT/τ ₀	2.3	8.24

699 Table 3. Definition and values of the dimensionless ratios Π in nature and in the experiments.

Exp	T (mm)	L _g (mm)	L _d (mm)	θ	α	T _t (mm)	σ (%)
1	10	16	116	58°	14°	15.5	55
2	10	14	105	63°	27°	15.4	54
3	30	42	150	58°	14°	37.7	27
4	30	48	138	56°	18°	41.2	37
5	50	58	164	58°	21°	53.7	7

700 Table 4. Measured (L_g, L_d, θ, α) and imposed (T) parameters in the experiments. T=overburden thickness; L_d= dome
701 diameter; L_g= apical depression width; θ= apical depression fault dip; α= dome flank mean dip; T_t= theoretical overburden

702 thickness calculated with equation 1 (Brothelände and Merle, 2015, see discussion section); σ = percentage difference between
703 T and T_c .